# Biological Control of Crystal Texture: A Widespread Strategy for Adapting Crystal Properties to Function

Amir Berman, Jonathan Hanson, Leslie Leiserowitz,
Thomas F. Koetzle, Stephen Weiner, Lia Addadi

Textures of calcite crystals from a variety of mineralized tissues belonging to organisms from four phyla were examined with high-resolution synchrotron x-ray radiation. Significant differences in coherence length and angular spread were observed between taxonomic groups. Crystals from polycrystalline skeletal ensembles were more perfect than those that function as single-crystal elements. Different anisotropic effects on crystal texture were observed for sea urchin and mollusk calcite crystals, whereas none was found for the foraminifer, *Patellina*, and the control calcite crystals. These results show that the manipulation of crystal texture in different organisms is under biological control and that crystal textures in some tissues are adapted to function. A better understanding of this apparently widespread biological phenomenon may provide new insights for improving synthetic crystal-containing materials.

Single crystals are widely used by organisms to provide stiffness and strength to their mineralized skeletal tissues. The crystals most commonly used for this purpose are composed of the calcium phosphate mineral, carbonate apatite, in the case of vertebrate skeletons and teeth, and the calcium carbonate minerals, calcite and aragonite, in the case of invertebrate exoskeletons. Most organisms use one of two different strategies for forming their crystals: growth occurs in a preformed matrix framework composed of macromolecules or in a preformed membrane-delineated vesicle. In the former case, the crystals are usually symmetrically shaped, expressing various crystal faces, and are often all aligned crystallographically. This results in a highly organized composite material composed of crystals embedded in an organic matrix. The major components of the matrix are usually relatively hydrophobic structural proteins or polysaccharides, such as type I collagen in vertebrate bones, or chitin associated with various proteins in mollusk shells and arthropod skeletons (*1*).

Skeletal tissues formed by crystal growth within vesicles usually result in crystals with complex, convoluted shapes and smooth and curved surfaces. Perhaps the most familiar group of animals that use this strategy for forming their mineralized skeletal components are the Echinodermata—the sea stars, brittle stars, sea cucumbers, and sea urchins. Many of their skeletons are composed of large unusually shaped single crystals of magnesium-bearing calcite, each of which is formed in a separate vesicle. The spines of sea urchins, some of which are tens of centimeters long, are each single crystals as determined by x-ray diffraction. Curiously, the five continuously growing teeth of sea urchins blend properties of both crystal-growing strategies. The individual crystals also each forms in a vesicle, but the final product is a highly organized multicrystalline array of high magnesium-calcite crystals in an organic matrix (*2*). Little is known about how calcareous sponges form their calcitic spicules. Based on the observations of Minchin (*3*) and Jones (*4*), the process appears to be similar to that used by echinoderms.

Almost all mineralized tissues, irrespective of the strategy used, contain a distinctive assemblage of unusually acidic proteins or glycoproteins or both (*1*). In some tissues, they are known to be intimately associated with the mineral phase, and many in vitro experiments show that they are capable of influencing crystal growth. They are therefore widely believed to be intimately involved in controlling crystal formation. It is also either generally believed, or perhaps more often implicitly assumed, that crystal components of mineralized tissues are basically the same as their inorganic counterparts. Here we provide unequivocal evidence that this is not the case for calcite crystals formed by both the matrix and the vesicle strategy. We show that a variety of organisms do exert control over the internal texture of their crystals. We suggest that one of the mechanisms used for achieving this is the controlled intercalation of some of the acidic macromolecules into the crystal lattice.

The assumption that biogenic and inorganic crystals are intrinsically the same has persisted, although it has been known for a long time that some skeletal elements behave crystallographically as single crystals, yet mechanically their behavior is more typical of amorphous materials. This behavior is true of calcitic spicules formed by sponges, echinoderm skeletal elements, and some unusual foraminiferal shells, all of which break with a conchoidal fracture, rather than the smooth planar cleavage surfaces characteristic of single inorganic crystals of calcite (*5*). The latter are known to be particularly brittle because of their tendency to readily cleave along the so-called "cleavage rhombohedron" planes ({104} in the hexagonal representation). Proposed explanations for the modified mechanical properties of the biogenic materials ranged from assuming a perfectly aligned assemblage of crystals (*6*) to suggesting that the conchoidal fracture is due to a shape-dependent reaction to mechanical stress (*7*). The presence of proteins inside crystals has been reported, but it was generally assumed that protein was trapped or deposited in the form of continuous sheaths between separate crystallites (*8*). We recently demonstrated that at least some of these proteins in sea urchin (echinoid) spines are dispersed inside the crystal lattice, so as to impart modified fracture properties to the single crystals (*9*). In this study, we compare the textures of a series of biogenic single calcite crystals of different origins.

## The Biogenic Calcite Crystals Examined

Figure 1 shows scanning electron micrographs of the seven types of biological calcite crystals from four different phyla that were examined. The range of shapes and sizes is enormous. They all fracture with conchoidal cleavage, except for the prisms of the mollusk shell *Atrina* (Fig. 1F) that tend to fracture along the cleavage planes of inorganic calcite (*10*). The mollusk prisms and the sea urchin tooth elements (Fig. 1G) both function as ordered multicrystalline arrays embedded in an or-

A. Berman, S Weiner, and L. Addadi are in the Department of Structural Biology and L. Leiserowitz is in the Department of Materials and Interfaces at the Weizmann Institute of Science, Rehovot 76100, Israel. J. Hanson and T. F Koetzle are in the Chemistry Department, Brookhaven National Laboratory, Upton, NY 11973

ganic matrix. At the other extreme, each entire spirillinid foraminifer shell (Fig. 1, D and E) is one single crystal (*11*), as is the adult sea urchin spine (Fig. 1A). The sea urchin larva is supported by two spicules (Fig. 1B), each one of which is a single crystal (*12*). The sponges (Fig. 1C) are intermediate in that the spicules are single-crystal elements that are not regularly organized in a matrix, but are usually densely packed in the tissue (*13*).

## Measuring Parameters of Crystal Texture

A six-circle Huber diffractometer, combined with a germanium (220) crystal analyzer on the detector arm, was used to collect series of diffraction peak profiles in the $\omega$ and $\omega/2\theta$ modes (*14*). As a resolution of a few thousandths of a degree was required, it was necessary to use well-collimated synchrotron x-ray radiation. The two scanning modes are related to two different parameters of crystal texture: mosaicity, or angular spread between the perfect crystal domains, and coherence length, or average dimension of the perfect domain. The angular spread is obtained directly from the $\omega$ profiles, and the coherence length is calculated from the $\omega/2\theta$ profiles applying the Scherrer formula (see legend of Fig. 2). Typically, one whole set of measurements included 10 to 15 diffraction peak profiles corresponding to planes (00*l*) [(006) and (0012)], (*hk*0) [(110) and (030)], and (*hkl*) [(104), (116), and (018)]. Diffraction was thus examined from various directions relative to the crystal axes. Some crystals, notably the sea urchin tooth element, were too small to allow collection of an entire data set. The experimental procedure and treatment of data are described in Figs. 2 and 3. The specifications and quality parameters of the data collected for each crystal are given in Table 1.

## Comparisons of Crystal Texture

The crystal textures of the biogenic elements are compared in Fig. 2, where they are expressed in terms of angular spread (ordinate) and the reciprocal of the coherence length (abscissa), averaged for each skeletal element over a series of reflections. Synthetic calcite crystals are also represented for reference. Each taxonomic group occupies a defined area of the graph. Thus measurements of the mollusk *Atrina* prisms are clustered together, as are the sponge spicules and the sea urchin *Paracentrotus* adult and larval spines. The two foraminifera are distinct one from the other and from the other skeletal elements. The major exception to this trend is the *Paracentrotus* tooth element.

In general, Fig. 2 shows that a higher mosaicity corresponds to a lower coherence length range, indicating that the two parameters of crystal perfection are not independent. There are, however, large deviations from linearity. The foraminifer *Spirillina*, for example, has a relatively large average coherence length, but an extremely broad angular spread, especially when compared to the sponge spicules that have similar values of coherence length. Thus the textural parameters cannot be trivially related to dislocations, that is, to a more perfect or less perfect mechanism of crystal growth.

The different skeletal elements have different magnesium contents, which may also affect crystal texture. Magnesium is usually

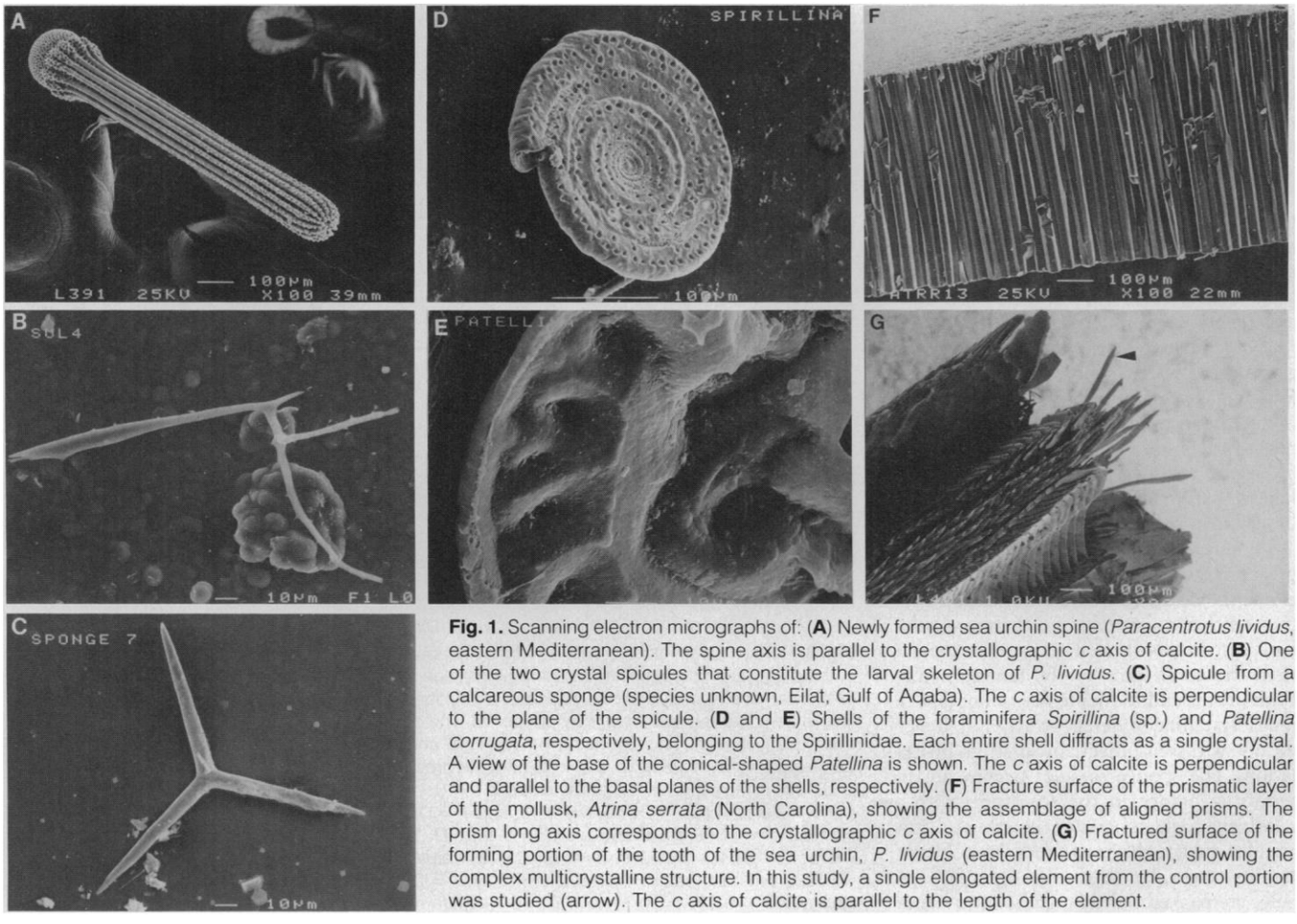


**Fig. 1.** Scanning electron micrographs of: (**A**) Newly formed sea urchin spine (*Paracentrotus lividus*, eastern Mediterranean). The spine axis is parallel to the crystallographic *c* axis of calcite. (**B**) One of the two crystal spicules that constitute the larval skeleton of *P. lividus*. (**C**) Spicule from a calcareous sponge (species unknown, Eilat, Gulf of Aqaba). The *c* axis of calcite is perpendicular to the plane of the spicule. (**D** and **E**) Shells of the foraminifera *Spirillina* (sp.) and *Patellina corrugata*, respectively, belonging to the Spirillinidae. Each entire shell diffracts as a single crystal. A view of the base of the conical-shaped *Patellina* is shown. The *c* axis of calcite is perpendicular and parallel to the basal planes of the shells, respectively. (**F**) Fracture surface of the prismatic layer of the mollusk, *Atrina serrata* (North Carolina), showing the assemblage of aligned prisms. The prism long axis corresponds to the crystallographic *c* axis of calcite. (**G**) Fractured surface of the forming portion of the tooth of the sea urchin, *P. lividus* (eastern Mediterranean), showing the complex multicrystalline structure. In this study, a single elongated element from the control portion was studied (arrow). The *c* axis of calcite is parallel to the length of the element.

considered to be homogeneously distributed inside the crystal lattice of calcite in the form of a solid solution, hence modifying the crystal lattice constants (*15*). It is expected, however, to introduce some stress in the lattice that would influence the ω spread and possibly also the coherence length of the crystal. There is also evidence, from morphological studies, that magnesium is introduced into synthetic calcite crystals preferentially through certain crystal planes (*16*). This effect could conceivably lead to higher concentrations of magnesium in distinct sectors within the crystal (*17*), but is unlikely to occur in those biologically formed crystals in which accretion occurs by continuous deposition of concentric circular layers, such as in the echinoderms and calcisponges. The magnesium contents, evaluated from the variation in calcite cell dimensions on a per mole basis, are 17% and 12% for the sponge spicules, 13% for *Spirillina*, 12% for *Patellina*, 7.5% for the *Paracentrotus* adult and larval spicules, 5.5% for the *Paracentrotus* tooth element, and is almost undetectable in the *Atrina* prisms. Neither of the two parameters, angular spread or coherence length, can be correlated with magnesium content. Thus magnesium is not the only contributing factor to the different values of texture.

We also note that the degree of mosaicity of the crystals cannot be related to crystal size or shape. The *Atrina* prisms are much larger than the *Paracentrotus* larval spicule and are in the same size range as the *Paracentrotus* adult spine (Table 1). Note too that the *Paracentrotus* larval spicule has a continuity of shape and is much less convoluted than the adult spine. Despite this, the spicule and spine have almost exactly the same range of mosaicity.

We conclude that the texture of each crystal type is an intrinsic property of the mineral lattice that varies from one taxonomic group to another. It cannot be only related to crystal size, shape, or the amount of magnesium. The possibility examined, here is that it may be related to the presence of occluded biological macromolecules.

In terms of crystal texture, the *Atrina* prisms are the most perfect biogenic skeletal elements measured and are most similar to the synthetic crystals. Furthermore, the *Paracentrotus* tooth element is more perfect than the adult spine or the larval spicule. Both prisms and tooth elements function in multicrystalline ordered arrays and hence do not withstand mechanical stress in isolation. The sponge spicules occupy an intermediate range in the spectrum, with a relatively high coherence length and low angular spread, close to that of the polycrystalline materials. In the sponge, the spicules are packed tightly together and hence

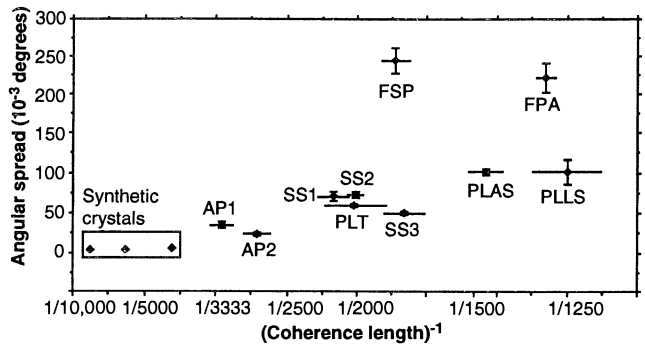


**Fig. 2.** Distribution of angular spread (ordinate) and reciprocal of the coherence length (abscissa) for the measured crystals, averaged over all of the measured profiles. In the box: synthetic crystals of pure calcite. The biogenic crystals are designated as follows: AP1 and AP2, *Atrina* prisms; SS1, SS2, and SS3, sponge spicules; PLT, *Paracentrotus lividus* tooth element; PLAS, *P. lividus* adult spicule; PLLS, *P. lividus* larval spicule; FSP, foraminifera *Spirillina* shell; and FPA, foraminifera *Patellina* shell. The angular spread was derived directly from the full width at half maximum (FWHM) of the peak profiles collected in the ω mode. The coherence length ($L$) was calculated from the Scherrer formula, $L = \lambda/\cos\theta \sqrt{B^2 - \beta^2}$ where $B$ is the peak width derived from the integrated intensity of the peak divided by its maximum intensity after subtracting the background level counts and β = instrumental resolution = 0.003 degrees. Derivations of FWHM directly from the peak width at half maximum agreed within 10%. Bars represent the standard error of the deviation. The diffraction data were collected at the National Synchrotron Light Source (Brookhaven National Laboratory) on beam line X7B (*14*).

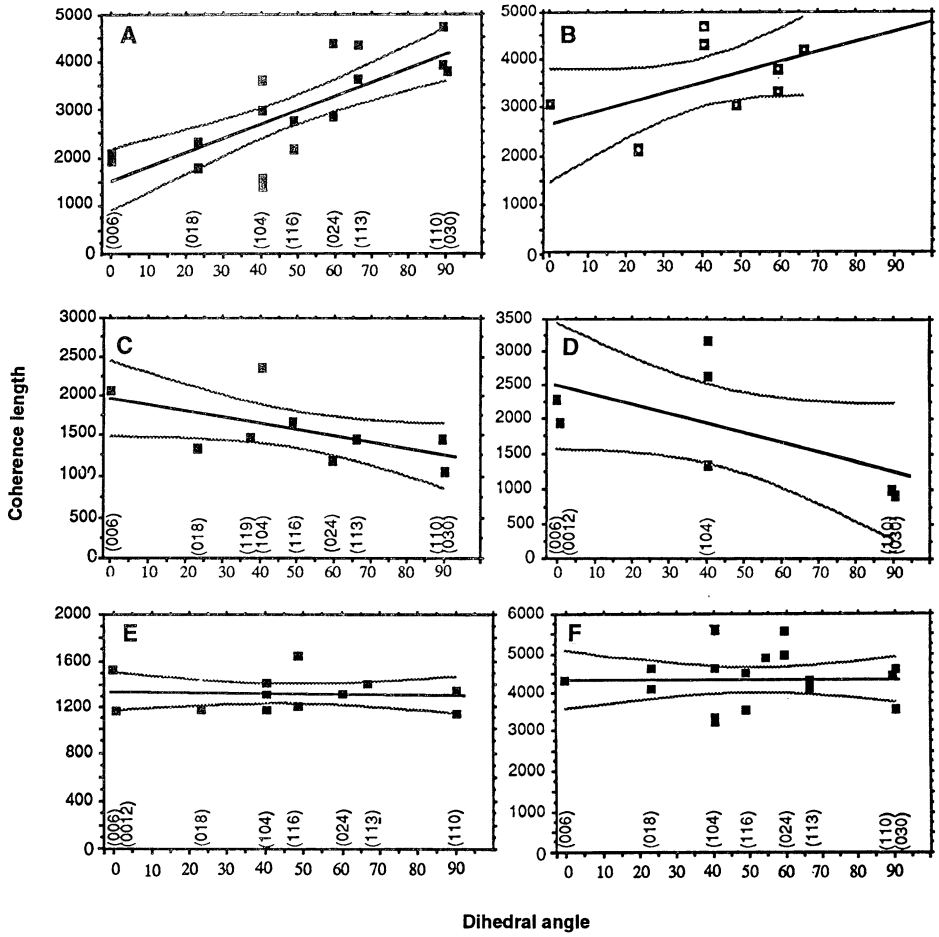


**Fig. 3.** Coherence lengths for different diffraction peaks of the same crystal, expressed as a function of the dihedral angle between the diffracting plane and the *ab* plane (001). The Miller indices of the reflections are indicated above the abscissa. Coherence lengths were calculated as in Fig. 2. The line is the linear regression of the data points. The curves delimit the 90% confidence bands for the true mean of $y$ (**A** and **B**) *Atrina* prisms AP2 and AP1, respectively. For AP2 the slope of the calculated linear regression is $s$ = 28.98 (Å/degree). The correlation coefficient is $r$ = 0.753, and $P$ = 0.0005 is the probability that the slope is $s$ = 0, based on the statistical F test. AP1 has the same general trend, with $s$ = 21.76, $r$ = 0.48, and $P$ = 0.159. (**C**) *Paracentrotus* adult spine (PLAS). The slope is $s$ = −7.99, $r$ = 0.566, and $P$ = 0 112. (**D**) The larval spicule (PLLS) shows the same trend, with $s$ = −13.81, $r$ = 0.59, and $P$ = 0.163. (**E**) *Patellina* shell (FPA); $s$ = 0.24, $r$ = 0.04, and $P$ = 0.89. (**F**) Pure synthetic calcite crystal 2; $s$ = 0.98, $r$ = 0.004, and $P$ = 0.99. For synthetic crystal 1, we obtained $s$ = 9.42, $r$ = 0.11, and $P$ = 0.76 (data not shown).

**Table 1.** Technical parameters of measurements. Number of data points was 100 in a given scan width except for those indicated by †, where $n = 150$. AP, *Atrina* prisms; SS, sponge spicules; PLAS, *Paracentrotus lividus* adult spicule; PLLS, *P. lividus* larval spicules; PLT, *P. lividus* tooth element; FPA, foraminifer *Patellina*; FSP, foraminifer *Spirillina*, and PC, pure calcite.

| Crystal | Size of crystal (μm) | | λ (Å) | Reflections collected (no.) | Range of intensities* (counts) | Width of scan (degrees) | |
|---|---|---|---|---|---|---|---|
| | Length | Width | | | | ω | ω/2θ |
| AP1 | 700 | 50 | 0.7912 | 15 | 221,000–1360 | 0.15 | 0.15 |
| AP2 | 700 | 50 | 0.7912 | 11 | 58,000–30 | 0.15 | 0.15 |
| SS1 | 70 | 10 | 0.9220 | 11 | 11,000–115 | 0.4 | 0.2 |
| SS2 | 70 | 10 | 0.9940 | 14 | 540–45 | 0.6† | 0.15 |
| SS3 | 70 | 10 | 0.9940 | 12 | 2,400–45 | 0.4 | 0.15 |
| PLAS | 800 | 700 | 0.945 | 17 | 2,150–160 | 0.3 | 0.3 |
| PLLS | 120 | 7 | 0.9220 | 7 | 350–30 | 0.5 | 0.25† |
| PLT | 300 | 10 | 0.945 | 2 | 1,000–600 | 0.25 | 0.25 |
| FPA | 100 | 10 | 0.9940 | 12 | 310–35 | 0.9† | 0.15 |
| FSP | 200 | 10 | 0.9940 | 16 | 14,500–660 | 0.9† | 0.15 |
| PC1 | 150 | 150 | 0.9940 | 10 | 18,000–960 | 0.15 | 0.15 |
| PC2 | 150 | 150 | 0.7912 | 16 | 250,000–220 | 0.15 | 0.15 |
| PC3 | 150 | 150 | 0.945 | 9 | 13,000–400 | 0.12 | 0.06 |

*The range of intensities refers to the peak maximum values for the different reflections †$n = 150$.

probably alter the mechanical properties of the tissue en masse (*13*). All of these observations strongly suggest that crystal texture is not only under biological control, but is somehow related to function.

The ability of extracted biological macromolecules from sea urchin skeletons to be selectively occluded within calcite crystals on planes parallel to the *c* axis and to influence crystal texture has been demonstrated in vitro (*9*, *14*). Presumably the changes observed in crystal texture in this study are related to the same phenomenon. If we assume that protein intercalation is directly related to the decrease in coherence length, the protein is intercalated in the sea urchin spine at intervals of 1500 to 2000 Å. In the mollusk shell element, on the other hand, the intracrystalline protein appears to be occluded at the boundaries of large domains (4000 to 5000 Å), similar in size to synthetic calcite (*10*). In vitro experiments in which proteins from *Atrina* prisms were used, resulted in non-specific interactions with growing calcite crystals, although these proteins were also occluded inside the crystals. Further experiments of this type with purified occluded proteins in the presence and in the absence of magnesium need to be performed to assess more precisely the role of the different proteins in controlling crystal texture.

## Anisotropy in Crystal Texture

Our interpretation of the mechanism of crystal reinforcement is based largely on the postulated effect on fracture of selective occlusion of protein along specific crystal planes parallel to the *c* axis but oblique to the cleavage plane (*9*). If this mechanism indeed operates in vivo, the proteins should induce relatively more textural disorder along planes parallel to the *c* axis as compared to planes oblique to the *c* axis. This disorder should be reflected at the level of crystal texture by preferential broadening of the diffraction peaks derived from the planes where adsorption took place, assuming that the occluded protein selectively or preferentially affects only the set of crystal planes where it was adsorbed. Here we report evidence demonstrating such an anisotropic effect.

In Fig. 3 we show the relations between the coherence length and the deviation of the diffracting plane from the *ab* plane for the two *Atrina* prisms, the *Paracentrotus* adult spine and larval spicule, the foraminifer *Patellina*, and one synthetic calcite crystal.

The control synthetic calcite crystals, as well as the foraminifer shell, show no discernible trend (Fig. 3, E and F; see legend for statistical analyses) (*18*). The *Paracentrotus* adult spine and larval spicule both show a small but significant decrease in coherence length along crystal planes parallel to the *c* axis (Fig. 3, C and D). This result implies that proteins are preferentially occluded on planes parallel to the *c* axis, and is consistent with the earlier morphological in vitro observations (*9*). The *Atrina* prisms show an opposite even more significant trend; the coherence length is preferentially decreased for planes perpendicular to the *c* axis (Fig. 3, A and B). Following our hypothesis, this would correspond to preferential occlusion of proteins on the *ab* plane. This result is in agreement with the presence in the prisms of well-developed growth lines in the same direction, as revealed by preferential etching. If this is correct, this observation may provide an important insight into the physical basis of such growth lines and an explanation for the manner in which they form.

This study shows that control over the textural properties of biologically formed crystals is a widespread phenomenon and that different organisms use different strategies for achieving this effect. It will be of much interest to decipher these strategies, learn more about the structural parameters that control various macromolecule-crystal interactions, and in so doing, possibly open the way to applying this new knowledge to manipulating crystal textures for the purposes of improving synthetic materials.

## REFERENCES AND NOTES


1. H. A. Lowenstam and S. Weiner, *On Biomineralization* (Oxford Univ. Press, New York, 1989); K. Simkiss and K. M Wilbur, *Biomineralization. Cell Biology and Mineral Deposition* (Academic Press, San Diego, 1989); L Addadi and S. Weiner, *Angew. Chem. Int. Ed. Engl.* **31**, 153 (1992).
2. P. Dubois and C. Chen, in *Echinoderm Studies*, M. Jangoux and J. M. Lawrence, Eds. (Balkema, Rotterdam, 1989), pp. 109–178.
3. E. A. Minchin, *Q. J. Microsc. Sci.* **52**, 301 (1908).
4. W. C. Jones, *Symp. Zool. Soc. London* **25**, 205 (1970)
5. _____ and D. F. James, *Micron* **3**, 196 (1972); H. Nissen, *Science* **166**, 1150 (1969), K. M. Towe, W. Berthold, D. E. Applemen, *J. Foraminiferal Res* **7**, 58 (1977); D. M. Raup, in *Physiology of Echinodermata* (Wiley, New York, 1966), p. 379; G. Donnay and D. L. Pawson, *Science* **166**, 1147 (1969).
6. K. M. Towe, *Science* **157**, 1048 (1967), P. L. O'Neill, *ibid.* **213**, 646 (1981).
7. R. B. Emlet, *Biol. Bull. Woods Hole Mass.* **163**, 164 (1982); J. D. Currey, *J Mar. Biol. Assoc. U.K.* **55**, 419 (1975); J. Weber, R Greer, B. Voight, E. White, R Roy, *J Ultrastruct. Res.* **26**, 355 (1969).
8. N. Watabe, *J. Cell. Biol.* **18**, 701 (1963); K. M. Towe and G. R. Thompson, *Calcif Tissue Res.* **10**, 38 (1972); H. Nakahara, M. Kakei, G. Bevelander, *Venus* **39**, 162 (1980).
9. A. Berman, L Addadi, S. Weiner, *Nature* **331**, 546 (1988).
10. L. Addadi, A. Berman, S. Weiner, *Mechanisms and Phylogeny of Mineralization in Biological Systems*, S. Suga and H. Nakahara, Eds. (Springer-Verlag, Tokyo, 1991), pp 29–33
11. A. Wood, *Q. J Geol. Soc. London* **104**, 229 (1949).
12. K Okazaki, *Embriologia* **5**, 283 (1960).
13. L. De Vos, K. Rutzler, N. Boury-Esnault, C. Donady, J. Vacelet, *Atlas of Sponge Morphology* (Smithsonian Institution, Washington, DC, 1991); M. A. R. Koehl, *J. Exp. Biol.* **98**, 239 (1982).
14. A Berman *et al.*, *Science* **250**, 664 (1990).
15. J. R. Goldsmith and D. L. Graf, *Am. Mineral.* **43**, 84 (1958), F. Lippmann, *Sedimentary Carbonate Minerals* (Springer-Verlag, Berlin, 1973).
16. J. O. Titiloye, S. C. Parker, D. J. Osguthorpe, S Mann, *J. Chem Soc Chem. Commun.* **20**, 1494 (1991).
17. For more information on the formation of sectors in crystal growth, see B. Kahr and J. M. McBride, *Angew. Chem. Int. Ed. Engl.* **31**, 1 (1992); I. Weissbuch, L. Addadi, M. Lahav, L. Leiserowitz, *Science* **253**, 637 (1991).
18. For additional data and discussion on the synthetic systems, see A Berman *et al.*, *J. Phys. Chem.*, in press.


19. We thank E. Holicz for providing us with the foraminifera, R. Dillaman for the *Atrina* shells, A Meroz for the sponge spicules, and B. Moav for the echinoderm larval spicules. Supported by grant 89-00148 from the U S.–Israel Binational Science Foundation. The research was carried out at Brookhaven National Laboratory under contract DE-AC02-76CH-00016 with the U S. Department of Energy, and supported by its Division of Chemical Sciences, Office of Basic Energy Sciences.